FEATURE-BASED TRANSFORMATION MODELS FOR SATELLITE IMAGE ORIENTATION AND TERRAIN MODELING

Ahmed Shaker
Institut de Geomatica, Generalitat de Catalunya & Universitat Politecnica de Catalunya
Parc Mediterrani de la Tecnologia, Av. del Canal Olimpic, E-08860 Castelldefels. Spain
Ahmed.shaker@ideg.es

ABSTRACT

The benefits from the use of the features attributes and the availability of different types of features on images (point- or linear-features) have raised the importance of using different feature-based transformation models for satellite image registration and terrain modeling. In the last decades, several research works have been conducted to facilitate the use of point- or linear-feature based transformation models for the satellite image orientation. However, most of these models depend on the availability of the sensor information (rigorous models) that may be withheld from user community. This research work presents a new form of the empirical 3D affine transformation model which can use either point- or linear-features for image registration and terrain modeling. The model is tested with different types of satellite sensors and the results show the applicability of the model with accuracy close to those from the rigorous models.

INTRODUCTION

For several decades, perspective geometry and projection has formed the basis of modelling the frame cameras. In this case, collinearity equations, as a rigorous model, describe the projection relation between the 2D image and the 3D object spaces. Unlike frame cameras, satellite imagery is based on line imaging techniques, where every line is imaged at different time. Therefore, precise knowledge of the satellite orbit, attitude, and camera alignments with respect to the spacecraft (satellite ephemeris data) are pre-required in order to apply the rigorous time-dependent mathematical models. With government-funded satellites, access to calibration and ephemeris data has allowed the development of the rigorous models. However, with regard to some of the new commercial high-resolution satellites, the satellite ephemeris data have been withheld from users, and therefore alternative empirical mathematical models have to be adopted.

Moreover, the use of the empirical mathematical models instead of the rigorous time-dependent mathematical models is sometimes more practical, despite the availability of the satellite information and the ephemeris data. This is because of the complexity to change the rigorous time-dependent mathematical model for different satellite sensors, the difficulties in selecting proper specialized software for multi-sensor triangulation (Madani, 1999), and the very long principal distance and the narrow angle of view, compared to the aerial photographs, that may make an orbital resection unstable (Li, et al. 2000).

In the last few years, there has been a substantial body of research work dealing with the use of point-based empirical mathematical models for the geometric correction of the new High-Resolution Satellite Imagery (HRSI). Different orders of Polynomials, Affine, Direct Linear Transformation (DLT), and Rational Function Models (RFM) are some of the models that have been used. Examples of the use of these models and the accuracy achieved can be found in Fraser et al., 2002; Grodecki, 2001; Fraser and Hanely, 2003; Shaker and Shi, 2003; Shi and Shaker, 2003; Tao and Hu, 2001.

In general, the point-based empirical mathematical models are used to link points in the image space and the corresponding points in the object space. However, under many circumstances accurately identifying discrete conjugate points may not be possible. Moreover, the lack of the control points in some remote areas such as deserts, forests, and mountainous areas provides a catalyst for the development of algorithms based on other image features. Unlike point features, which must be explicitly defined, linear features have the advantage in that they can be implicitly defined by any segment along the line.

In the era of digital imagery, using linear features has become an advantage due to several factors that can be summarized as follows: a) Linear features can be easily identified in the image by many automatic extraction tools and in object space; they can be obtained from an existing GIS database, hardcopy maps, and terrestrial mobile mapping systems (using, for instance, kinematic GPS techniques); b) It is easier to implement an automatic feature extraction algorithm instead of extracting point features, since linear features have more attributes than point features; c) Information from linear features can be used even without a complete match between image and object linear features; d) Linear features can be presented by either a set of points on the feature or a set of feature descriptors, which means that many geometric constraints and additional information

can be contributed to the solution (Kanok, 1995); and finally, e) linear features add more information, increase redundancy, and improve the geometric strength of adjustment (Habib et al., 2003).

Some efforts have been made to use linear features in different models for frame and linear array scanners (see Kanok, 1995; Habib et al., 2003; Mulawa and Mikhail, 1988; Habib et al., 2003; Dare and Dawman, 2001; Tommaselli and Tozzi, 1996). However, there are several limitations in applying some of these models due to: a) the availability of the required sensor and system information that are withheld from some of the HRSI user community; b) the validity of the models for the projective geometry, which is not exactly the case for linear array sensor imagery; and c) Numerical problems that could be encountered because of the initial approximation.

From the previous research work, linear features have been used successfully in rigorous mathematical models and point features have been used successfully in empirical mathematical models. This work tries to address the case where both satellite information and point control features are absent by developing a new form of the 3D affine model named "the 3D Affine Line-Based Transformation Model (ALBTM)", which is an empirical mathematical model that can use linear features and/or point features as control features for satellite image orientation and 3D geo-positioning.

THE 3D AFFINE LINE BASED TRANSFORMATION MODEL (ALBTM)

The successful exploitation of linear features for image orientation requires consideration of two major aspects: first, the mathematical description of the linear features in the image and the object spaces; and second, the mathematical representation of the relationship between the two spaces. For the first aspect, linear features can be presented in both image and object spaces in different ways. Straight lines, circles, ellipses and free-form lines are examples of such representation. In this work, straight lines as well as natural lines (free-form lines) converted to straight lines by mathematical functions are considered. Circles and ellipses are discarded because they are impractical and not transformation invariant.

For the second aspect, several assumptions are adopted to circumvent the complexity of the time-dependent mathematical models and to simplify the relationship between the image and the object spaces. These assumptions are: a) the satellite sensor moves linearly in space in a stable attitude, b) the sensor orientation angles are constant, and c) the satellite flight path is almost straight. It is important to mention that these assumptions are valid for a proportionally small coverage area, where the scan and the orbital velocity vectors are approximately aligned, and there is a very little change of the sensor elevation angle. This is, for instance, the case for the most typically scanning mode of Ikonos (Reverse mode). For Forward scanning mode of Ikonos and with the scanning mode of Quickbird, these assumptions may need to be revised (Fraser and Yamakawa, 2004).

Under these assumptions, the scanned lines by the sensor can be considered to form a continuous image for a small area. Based on that, the relationship between the image and the object spaces, which used to be presented by the collinearity equations, can be presented by simple affine transformation relations similar to those introduced in Fraser et al., 2003; Shaker and Shi, 2003; Shi and Shaker, 2003; and Fraser and Yamakawa, 2004.

On this basis, the underlying principle of the developed model is that the relationship between the unit vector components of line segments on linear features in the image space and the object space can be expressed in an affine transformation relationship. The model adopts the same structure for 3D transformation as the eight-parameter affine model. Adopting this structure allows us to use the same coefficients of the point and the line-based affine model for image orientation. The 3D ALBTM can be derived mathematically by locating any two points on a line segment in the image space and in the object space. The points located on the line segments in the image and the object spaces are not conjugate points but the line-segments they laid on are conjugate lines. Details of the derivation of the 3D ALBTM is presented in Shaker and Shi, 2007; and reference to it is in the following section.

Derivation of the 3D ALBTM

The 3D ALBTM is derived by performing the relationship between vectors $\vec{v}_{12}$ and $\vec{V}_{12}$, which are the unit vectors of the conjugate line segments in the image and the object spaces (Figure 1). The two unit vectors can be defined by any two points along the line segment in the image and the object spaces and can be presented in the matrix form as follows.

$$\vec{v}_{12} = \begin{bmatrix} a_x & a_y & 0 \end{bmatrix}^T$$

where:

$a_x = \frac{x_2 - x_1}{\sqrt{(x_2 - x_1)^2 + (y_2 - y_1)^2}}$, $a_y = \frac{y_2 - y_1}{\sqrt{(x_2 - x_1)^2 + (y_2 - y_1)^2}}$ and (x_1, y_1), (x_2, y_2) are the image coordinates of any two points along the line segment in the image space.

and $\vec{V}_{12} = [A_X \quad A_Y \quad A_Z]^T$

where:

$A_x = \frac{(X_2 - X_1)}{\sqrt{(X_2 - X_1)^2 + (Y_2 - Y_1)^2 + (Z_2 - Z_1)^2}}$, $A_y = \frac{(Y_2 - Y_1)}{\sqrt{(X_2 - X_1)^2 + (Y_2 - Y_1)^2 + (Z_2 - Z_1)^2}}$, $A_z = \frac{(Z_2 - Z_1)}{\sqrt{(X_2 - X_1)^2 + (Y_2 - Y_1)^2 + (Z_2 - Z_1)^2}}$, and ($X_1$, Y_1, Z_1) and (X_2, Y_2, Z_2) are the object (ground) coordinates of any two points along the line segment in the object space.

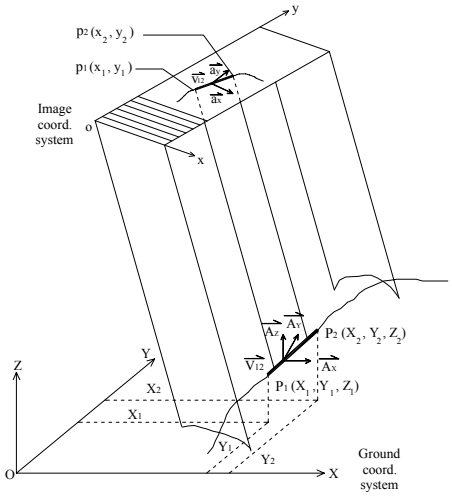

Figure 1. Representation of line unit vectors in the image and object spaces.

Let us start from assuming that the coordinates of any two points (p_1 and p_2) along a line segment in the image space are $p_1 = (x_1, y_1)$ and $p_2 = (x_2, y_2)$, and their corresponding coordinates in the object space are $P_1 = (X_1, Y_1, Z_1)$ and $P_2 = (X_2, Y_2, Z_2)$. Then the ordinary point-based eight-parameter affine transformation model can be presented for the points P_1 and P_2 as follows.

For point P_1:

$$x_1 = C_1 X_1 + C_2 Y_1 + C_3 Z_1 + C_4 \quad (1)$$

$$y_1 = C_5 X_1 + C_6 Y_1 + C_7 Z_1 + C_8 \quad (2)$$

For point P_2:

$$x_2 = C_1 X_2 + C_2 Y_2 + C_3 Z_2 + C_4 \quad (3)$$

$$y_2 = C_5 X_2 + C_6 Y_2 + C_7 Z_2 + C_8 \quad (4)$$

where (x_1, y_1) and (x_2, y_2) are the image coordinates of the points p_1 and p_2 , (X_1, Y_1, Z_1) and (X_2, Y_2, Z_2) are the corresponding object (ground) coordinates of the two points, and C_1, C_2,…, C_8 are the model coefficients.

Subtracting equation (1) from (3),

$$x_2 - x_1 = [C_1 X_2 + C_2 Y_2 + C_3 Z_2 + C_4] - [C_1 X_1 + C_2 Y_1 + C_3 Z_1 + C_4] \quad (5)$$

Then,

$$x_2 - x_1 = C_1(X_2 - X_1) + C_2(Y_2 - Y_1) + C_3(Z_2 - Z_1) \quad (6)$$

Similarly subtracting equation (2) from (4) can lead to the following equation,

$$y_2 - y_1 = C_5(X_2 - X_1) + C_6(Y_2 - Y_1) + C_7(Z_2 - Z_1) \quad (7)$$

Dividing equations (6) and (7) by $l_{12} = \sqrt{(x_2 - x_1)^2 + (y_2 - y_1)^2}$, which is the length of the line segment on the image performed by connecting points p_1 and p_2, we get the following equations

$$\frac{x_2 - x_1}{l_{12}} = C_1 \frac{(X_2 - X_1)}{l_{12}} + C_2 \frac{(Y_2 - Y_1)}{l_{12}} + C_3 \frac{(Z_2 - Z_1)}{l_{12}} \quad (8)$$

$$\frac{y_2 - y_1}{l_{12}} = C_5 \frac{(X_2 - X_1)}{l_{12}} + C_6 \frac{(Y_2 - Y_1)}{l_{12}} + C_7 \frac{(Z_2 - Z_1)}{l_{12}} \quad (9)$$

Multiplying the right hand side of equations (8) and (9) by $\frac{L_{12}}{L_{12}}$,

where $L_{12} = \sqrt{(X_2 - X_1)^2 + (Y_2 - Y_1)^2 + (Z_2 - Z_1)^2}$, which is the length of the corresponding line segment on the ground. Equations (8) and (9) can be presented as follows

$$\frac{x_2 - x_1}{l_{12}} = C_1 \frac{(X_2 - X_1)}{L_{12}} \times \frac{L_{12}}{l_{12}} + C_2 \frac{(Y_2 - Y_1)}{L_{12}} \times \frac{L_{12}}{l_{12}} + C_3 \frac{(Z_2 - Z_1)}{l_{12}} \times \frac{L_{12}}{l_{12}} \quad (10)$$

$$\frac{y_2 - y_1}{l_{12}} = C_5 \frac{(X_2 - X_1)}{L_{12}} \times \frac{L_{12}}{l_{12}} + C_6 \frac{(Y_2 - Y_1)}{L_{12}} \times \frac{L_{12}}{l_{12}} + C_7 \frac{(Z_2 - Z_1)}{l_{12}} \times \frac{L_{12}}{l_{12}} \quad (11)$$

A close look to the left hand side of the equations (10) and (11) shows that the left-hand side of the two equations [$\frac{x_2 - x_1}{l_{12}}$ and $\frac{y_2 - y_1}{l_{12}}$ terms] are the unit vector components of the line segment connecting points p_1 and p_2 in the image space (a_x and a_y). Also, the terms [$\frac{(X_2 - X_1)}{L_{12}}$, $\frac{(Y_2 - Y_1)}{L_{12}}$, $\frac{(Z_2 - Z_1)}{L_{12}}$] in the right hand side of the equations (10) and (11) are presenting the unit vector components of the corresponding line segment in the ground space (A_X, A_Y, A_Z). It is important to mention that the unit vector components of any line segment can be determined from coordinates of any two points along the line segment. Therefore, the points used to determine the unit vector of the line segment in the image space and the object space may not be conjugate points but the lines they laid on are conjugate lines.

Substitute a_x, a_y, A_X, A_Y, A_Z in equations (10) and (11), the following two equations can be formulated

$$a_x = \frac{L_{12}}{l_{12}}[C_1 A_X + C_2 A_Y + C_3 A_Z] \quad (12)$$

$$a_y = \frac{L_{12}}{l_{12}}[C_5 A_X + C_6 A_Y + C_7 A_Z] \quad (13)$$

Sending $\frac{L_{12}}{l_{12}}$ from the right-hand side to the left-hand side of the equation, then equations (12) and (13) can be written as follows:

$$\frac{l_{12}}{L_{12}} a_x = C_1 A_X + C_2 A_Y + C_3 A_Z \quad (14)$$

$$\frac{l_{12}}{L_{12}} a_y = C_5 A_X + C_6 A_Y + C_7 A_Z \quad (15)$$

Substitute $\frac{l_{12}}{L_{12}}$ by S_i, then, the final form of the 3D ALBTM can be presented by the following two equations

$$S_i a_x = C_1 A_X + C_2 A_Y + C_3 A_Z \quad (16)$$

$$S_i a_y = C_5 A_X + C_6 A_Y + C_7 A_Z \quad (17)$$

where (a_x, a_y) are the unit vector components of the line segments in the image space, (A_X, A_Y, A_Z) are the unit vector components of the line segments in the object (ground) space, S_i is a local scale factor between each line segment defining a line in the image and the object spaces, and $C_1, C_2, \ldots, C_7$ are the model coefficients. It is worth mentioning that points defining the line segments in the image and the object spaces are not conjugate points since the unit vector components can be calculated using any two points along the line segment, but the line segments the points located on should be on conjugate lines.

Using the 3D ALBTM

The form of the 3D ALBTM is similar to the form of the 3D affine point-based transformation model. The difference is in the use of the unit vector components of the line segments (as control features) instead of the point coordinates in order to calculate the rotation and the scale coefficients of the model ($C_1, C_2, C_3, C_5, C_6, C_7$). These coefficients are similar to the coefficients of the 3D affine point-based transformation model since the form of the 3D ALBTM is delivered from the form of the 3D affine point-based transformation model. However, the translation coefficients (C_4 and C_8) do not appear in the form of the 3D ALBTM because the unit vector does not provide a unique representation of a line when the unit vector presents the line in question and any parallel line. Therefore, the 3D ALBTM expresses the relationship between a group of lines in the image space and any other parallel group of lines in the object space.

Generally, the translation coefficients can be determined by using one Ground Control Point (GCP) with the original form of the point-based 3D affine transformation model or by knowing the shift between the origins of the image and the object space coordinate systems (this is a special case, which can be used only when local image and object coordinate systems are used). There is no doubt that more than one GCP could be used to recover the translation coefficients; however, one point is sufficient.

Similar to conventional photogrammetry, both the line- and the point-based 3D affine model can be applied consecutively in space resection operation to calculate the coefficients of the model (the image transformation parameters) and space intersection operation to determine the coordinates of any point on the ground (when using stereo images). Generally, at least three line segments (here we called the line segments the Ground Control Lines (GCLs)) can be used to determine the rotation and the scale coefficients of the model. Following that, and by the aid of one control point, the translation coefficients can be determined. Finally, the original form of the 3D affine point-based transformation model can be used to calculate the ground coordinates of any point (in case of using stereo images) in the area covered by the images.

Synthetic as well as real data sets have been used to check the validity of the new approach and a comparative study has discussed the effectiveness and the limitations of the new model. The following section demonstrates representative sets of the results of the experimental work from two different real data sets.

EXPERIMENTAL WORK

Data Sets

Two different data sets from different satellite sensors have been used. The first dataset includes a SPOT 4 Panchromatic (PAN) stereo pair images in 10 m resolution covering the east part of Cairo province in Egypt. The images cover an area of about 50 x 40 km^2. The western part of the area covered by the images is nearly flat, while the remaining parts are hilly with a difference in ground elevation of about 450 m. Many linear and point features could be easily recognized on the images to be used as GCLs and checkpoints. The linear features were roads, highways and some water canals, while the point features were well-known road intersections, road-canal intersections, and pavement corners.

A kinematic GPS technique was used to observe the linear features in the field. Observations of the roads and the highways were made by putting a GPS antenna on the top of a Van and driving along the roads and the highways. In total, thirty well-distributed GCLs (line segments) were extracted from the kinematic GPS observations. Thirty-one checkpoints distributed on the entire area covered by the images are also observed by the fast static GPS technique. The analyses and the adjustments of the GPS data show that the ground accuracy of the GCLs and the checkpoints was within 5 cm in the horizontal directions and 9cm in the vertical one. However, the identification accuracy of the GCLs and the checkpoints are estimated to be within two-to-three pixels.

The low accuracy of the identification of the GCLs and the checkpoints on the images are mainly because of the low resolution of the images and the conditions of the ground observation which makes the identification process of the exact location of the Van on the image is a difficult task. This identification problem appeared especially on the highways where the exact lane (the Van was driven in) was difficult to be identified. The same identification problem with the checkpoints was recorded when it was difficult to determine the exact location of the van in each intersection. More information on the image specifications and the data set conditions can be found in Barakat et al., 2002; and Shaker, 2007. Figure 2 shows the distribution of both the GCLs and the checkpoints on the area covered by the images.

The second dataset is a stereo pair images from IRS/1D satellite covering 71x79 km^2 of a part of western desert in south Egypt. The two images of stereo have an overlap of about 84% and viewing directions of +19.59° and –19.74° against the nadir, which led to 0.76 Base-to-Height ratio (B/H). The images are PAN with resolution of 5.8 m which were resampled to 5.0 m. The area covered by the images is near to flat where the elevation difference is about 320 m along the study area. Details of the image specifications and the study area can be found in Shaker et al., 2003

As a part of the western desert, no old topographic maps were available for the study area that may help for extracting the GCLs or the checkpoints. Therefore, a survey mission was carried out before the satellite scanned the area to establish new artificial ground points to be used as checkpoints. The size of the points was selected taking into consideration the spatial resolution of the satellite (5.8m). Details of the specifications of the artificial ground points have been published in Shaker et al., 2003.

A GPS survey mission was conducted using fast static GPS technique where a total number of 21 ground points were observed including the main highway intersections. The center of each of the artificial points was located and the highway intersections were precisely observed. Moreover, all roads in the area covered by the images were also observed by the kinematic GPS technique similar to the work done for Cairo SPOT 4 data set. The configurations of the GCLs and the checkpoints observed by the GPS are shown in Figure 3. Both the accuracy of the GPS observation-adjustments and the point identifications on the image were estimated to be about 10 cm and half pixel, respectively.

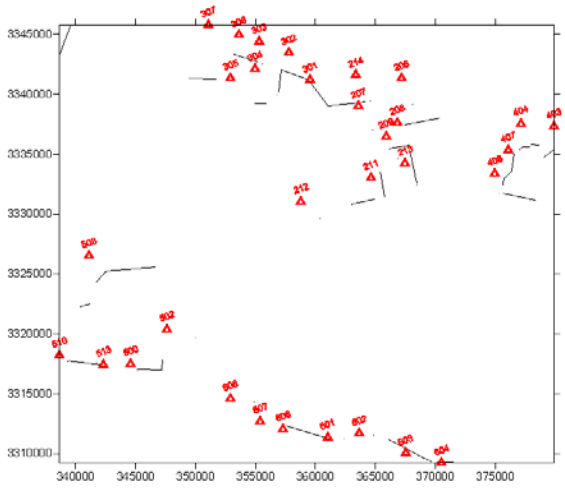

Figure 2. Distribution of the GCLs and the Checkpoints on the area covered by Cairo SPOT 4 Stereo pair

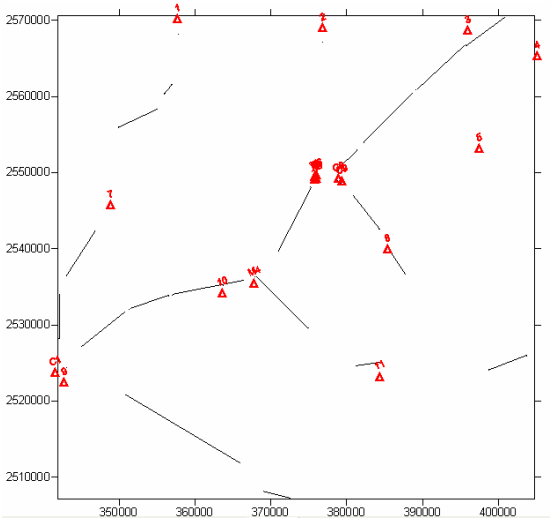

Figure 3. Distribution of the GCLs and the Checkpoints on the area covered by South Egypt IRS Stereo pair

Results and Analysis

Generally, the procedure of the work is divided into two steps: a) calculations of the image parameters (the coefficients of the affine transformation model) for each image of the stereo individually by the aid of the GCLs, one control point, and the least squares adjustment in a resection process, and b) determinations of the ground coordinates of any point in the area covered by the stereo images using the model coefficients and the image coordinates of the point on the two images in an intersection process.

As explained in section 2, the unit vector components of the GCLs were calculated using any two points along each line-segment in the image and the object spaces. The two points on the line-segment in the image space are not conjugate with the two points on the line-segment in the object space, but the lines they located on are conjugate lines. Then, the coefficients of the 3D ALBTM were determined for each image of the stereo pair using the unit vector components of the GCLs and equations (16 and 17). Based on that, the six coefficients related to the scale and the rotations were defined and the remaining two translation coefficients in the original form of the point-based 3D affine model are determined using one GCP.

Different numbers of well-distributed GCLs were used and the results from both SPOT 4 and IRS-1D data sets are presented in Figure 4 and 5. The results are presented in pixels for the RMS errors of the independent checkpoints in the X, Y and Z directions. The accuracy of the results is presented in pixels in order to compare between accuracies obtained from different satellite sensors in different resolutions. Applying the 3D ALBTM to SPOT 4 data set and using four-to-thirty well-distributed GCLs, the RMS errors of the checkpoints was varied from 39.65-to-3.98, 36.74-to-5.97, and 24.16-to-7.39 pixels in the X, Y, and Z directions, respectively. Using IRS-1D data set and four-to-nineteen well-distributed GCLs, the accuracy achieved was varied from 10.49-to-4.40, 6.55-to-3.93, and 5.05-to-3.83 pixels in the X, Y, and Z directions, respectively.

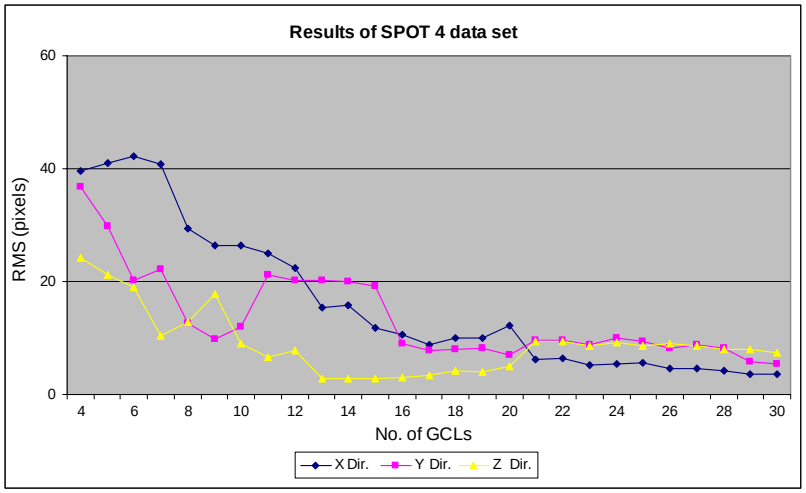

Figure 4. Results of SPOT 4 data set

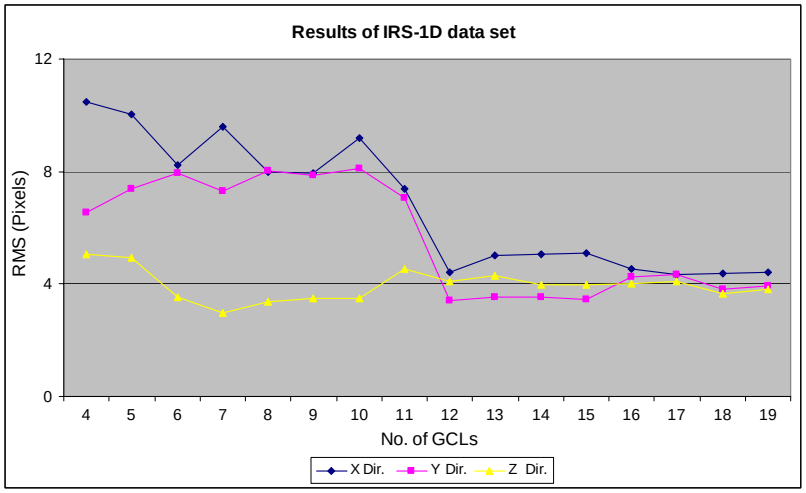

Figure 5. Results of IRS-1D data set

The results indicate that the 3D ALBTM could be used to determine the image scale and orientation parameters but several remarks from the results can be recorded. First, increasing the number of the GCLs increases the accuracy of the results in most of the cases when the GCLs were well distributed over the area covered by the images (well-planimetric and -elevation distribution). However, in some cases the results were deteriorated by increasing the number of the GCLs. Second, the accuracy of the results obtained from the IRS-1D data set was better than the accuracy achieved from the SPOT 4 data set. Third, the accuracy achieved using the 3D ALBTM was slightly worse comparing to the accuracy achieved using the point-based affine model.

Investigating different factors that might affect the performance of the model and might deteriorate the accuracy of the results, one can consider the effects from: a) the size of the coverage area and the errors related to the Earth curvature, b) effects from the characteristics of the GCLs (the lines direction, inclination angle, length, and slope), and c) effects from the accuracy of the control data. In this test, effect from the Erath curvature and the area size can be neglected because a single stereo pair and the UTM projected frame reference were used which minimize the errors related to the area size and the coordinate system.

Characteristics of the GCLs were studied using the simulated data and it was found that the line slope, which is also a function of the line length, and the vertical-horizontal distribution of the GCLs have considerable effect on the accuracy of the results. Lines having low slope performed better than lines with higher slope, and generally the lines should be well-distributed in both horizontal and vertical directions. In this work, most of the line slopes were low and they were well distributed on the area covered by the images.

Referring to the effect from the accuracy of the control data, the manner the point-based affine model handling errors has been studied in photogrammetry especially for the interior orientation process (see Fryer et

al. 1993 and Fraser, 1982). It was found that the affine transformation model distributes any observation error equally on all other observations and therefore the apparent size of error of any adjusted observation is minimized. However, it was found that the relative shape and the geometry of the image are distorted after the transformation process. Therefore, in case of any gross error in the identification of one or more of the observations (the GCPs in that case), the affine model distributes the gross error on all other observations. As a result, the relative shape and the image geometry are distorted and the overall accuracy is declined.

This manner of the point-based affine model in dealing with errors is similar to the manner the 3D ALBTM handle errors. This may emphasize the reason behind the higher accuracy from the IRS-1D data set comparing to the accuracy from SPOT 4 data set, which contains an estimated identification errors of about 2-3 pixels in both of the GCLs and the checkpoints as was indicated in section 3.1. The effect of the accuracy of the control data is also obvious in Figure 4 when the accuracy of the results is perturbed using different numbers of GCLs depending on the accuracy of each GCL used in the test.

All the previous factors, which were discussed above, may have an influence on the performance of the model to some extent and may affect the accuracy of the results. However, under the special conditions of the SPOT 4 data set, we expect that the identification error of the GCLs and the checkpoints had a significant rule on the overall accuracy achieved. Generally, the results achieved illustrate that four pixels of accuracy can be achieved in the X, Y and Z directions using a modest number of accurate and well-distributed GCLs. Similar to other empirical models, the 3D ALBTM is influenced by the control data. The more accurate the control data is, the better accuracy that can be achieved.

CONCLUSIONS

This paper presents the 3D Affine Line-Based Transformation Model (ALBTM) for satellite image orientation and terrain modeling. The underline principle of the model is that the point coordinates in the representation of the ordinary affine point-based transformation model can be replaced by the line unit vector components of line-segments on the linear feature. Any two points along a line-segment could be measured to calculate the line unit vector components. The two points measured on the line segment in the image and object spaces are not required to be conjugate points, but the line-segments they located on are required to be segments of conjugate lines.

In this work, real data has been used to test the developed model, and the results show that the model is applicable for the orientation and terrain modeling of HRSI. In particular, accuracy in terms of few pixels of RMS errors could be achieved. From the results obtained and based on the assumptions of the model, we found that the GCLs used in the developed model should be in low slopes, accurate, and well distributed over the area covered by the stereo images. Considering the control line characteristics and accuracy, the results obtained using the ALBTM are found to be close to those obtained by using other point-based empirical mathematical models.

In current research, consideration is given to other forms of the empirical mathematical models such as polynomial model, which could be modeled as the ALBTM. The ALBTM developed in this paper is also used for image-to-image and image-to-map registration.

ACKNOWLEDGMENTS

The author would like to acknowledge the support grand from the European Commission, the Sixth Framework Program, the Marie Curie International Incoming Fellowship under which the experimental work is done and the paper is written. The author would like to thank Prof. John Shi and Dr. IZ Huseyin Baki for their constructive discussions during the development process of the model. Also, the author is grateful to Dr. Ismael Colomina for his valuable comments. The acknowledgments are also extended to the Hong Kong Polytechnic University for their support (project no. G-YX61) during the development of the model.

REFERENCES

Barakat, H., ElAshmawy, N., and Shaker, A., 2002. Comparison between approximate and rigorous mathematical modeling for stereo SPOT imagery. *Journal of Civil Engineering*, Al Azhar University (CERM), Vol. 24, No. 4, pp. 1131 – 1147.

Dare, P., and Dowman, I., 2001. An improved model for automatic feature-based registration of SAR and SPOT images. *ISPRS Journal of Photogrammetry and Remote Sensing*, 56 (1): 13-28.

Fraser, C. S., Baltsavias, E. and Gruen, A., 2002. Processing of IKONOS imagery for sub metre 3D positioning and building extraction, *ISPRS Journal of Photogrammetry and Remote Sensing*, 56(3): 177-194.

Fraser, C.S., and Hanely, H.B., 2003. Bias compensation in rational functions for Ikonos satellite imagery. *Photogrammetric Engineering and Remote Sensing*, 69(1): 53-57.

Fraser, C.S., and Yamakawa, T., 2004. Insight into the affine model for high-resolution satellite sensor orientation. *ISPRS Journal of Photogrammetry & Remote Sensing*, 58 (2004): 275-288

Fraser, C. S., 1982, Film unflatness effects in analytical non-metric photogrammetry, *International Archives of Photogrammetry*, 24(5), pp. 156-166

Fryer, J. G., 1993, Affine or conformal? Fiducials or not!. Australian Journal of Geodesy, *Photogrammetry and Surveying*, 58(June), pp. 23-35

Grodecki, J., 2001. Ikonos stereo feature extraction—RPC approach. *Proceedings of ASPRS Annual Conference*, 23-27 Aprl, St. Louis, Missouri. (http://www.spaceimaging.com/whitepapers_pdfs/2001/IKONOS%20Stereo%20Feature%20Extraction-ASPRS%202001.pdf).

Habib, A.F., Lin, H.T., and Morgan, M.F., 2003. Line-based modified iterated Hough transform for autonomous single-photo resection. *Photogrammetric Engineering and Remote Sensing*, 69(12): 1351-1357

Kanok, W., 1995. Exploitation of linear features for object reconstruction in digital photogrammetric systems. PhD thesis, Purdue University.

Li, R., Zhou, G., Yang, S., Tuell, G., Schmidt, N. J. and Flower, C., 2000. A study of the potential attainable geometric accuracy of IKONOS satellite imagery. *International Archives of Photogrammetry and Remote Sensing*. 33(B4): 587-595.

Madani, M., 1999. Real time sensor-independent positioning by rational functions, Direct versus indirect methods of sensor orientation. *Workshop of ISPRS*, Barcelona, November 1999, pages: 64-75.

Mulawa, D. C., and Mikhail, E. M., 1988. Photogrammetric treatment of linear features. *Proceedings of the XVIth Congress of ISPRS*, Commision III, 27(part B10), ISPRS, Elsevier, Amsterdam, The Netherlands, pages: 383-393.

Shaker, A., Shi, W. Z, and Emam, H., 2003. The use of empirical methods in topographic map production of IRS-1D images. *Proceedings of the Annual Conference ASPRS*, Anchorage, USA, on CD ROM.

Shaker, A., and Shi, W. Z, 2003. Polynomial models as a tool for mapping high-resolution satellite imagery. *Proceedings of European remote sensing conference (SPIE)*, 9-11 September, Barcelone, Spain, pages: 224-233

Shaker, A., and Shi, W. Z, 2007. Method of satellite image orientation using Affine Lined-Based Transformation Model. Patent application file No. 200710002098.4.

Shaker, A., 2007. Satellite sensor orientation and 3D geo-positioning using empirical models. *International Journal of Applied Earth observations and geoinformation*, (submitted).

Shi, W. Z, and Shaker, A., 2003. Analysis of Terrain Elevation Effects on IKONOS Imagery Rectification Accuracy by Using Non-Rigorous Models. *Photogrammetric Engineering and Remote Sensing*, 69,(12): 1359-1366

Tao, C.V., and Hu, Y., 2001. A comprehensive study of the rational function model for photogrammetric processing. *Photogrammetric Engineering and Remote Sensing*, 67(12): 1347-1357.

Tommaselli, A.M.G., and Tozzi, C.L., 1996. A Recursive approach to space resection using straight lines. *Photogrammetric Engineering and Remote Sensing*, 62(1): 57-66